J Mater Sci (2008) 43:1701–1710
DOI 10.1007/s10853-007-2358-3

Phase composition and wear behavior of NiTi alloys

Stefano Gialanella · Gloria Ischia · Giovanni Straffelini

Received: 16 July 2007 / Accepted: 27 November 2007 / Published online: 11 January 2008

Abstract This study deals with the wear behavior of two NiTi shape memory alloys, one of them being martensitic, the other one austenitic at room temperature. Wear tests have been conducted with a disk-on-block geometry. The block was made of the NiTi alloy, whereas counterface disk materials were AISI M2 high-speed steel and a WC–Co hardmetal. From the evolution of the friction coefficient and temperature during the tests and from the characterization of the wear debris and traces, it has been possible to identify the main wear mechanisms. In the wear tests involving the M2 steel disk, both NiTi alloys display a transition, as a function of the applied load, from a mainly oxidation regime to a more complex situation, in which oxidation wear is accompanied by delamination of metallic alloy fragments. Higher wear rates of the shape memory alloys have been observed for the NiTi/WC–Co coupling. In this case, a transition from a mainly delamination wear to a regime featuring a mixture of delamination and oxidation wear has been observed.

Introduction

In the class of shape memory alloys (SMAs), NiTi materials definitely have a central role. A very large number of research works, aiming at understanding the main aspects of the shape memory effect (SME) and pseudoelasticity (PE) have been carried out over the years using NiTi alloy specimens. Moreover, these alloys, either in binary or more complex compositions, are used in most of the commercial and technological applications of SMAs [1, 2]. The reasons for this success can be found in the wide range of interesting properties displayed by these materials, that render them suitable for a wide range of different applications. Just to mention the main fields in which NiTi alloys have been profitably employed, we remind biomedical applications [3], for which, incidentally, the presence of nickel turned out not to be a problem, as no release of this potentially allergenic element was detected [4, 5], aerospace deployment systems [6], safety devices [7], actuators and robotics [8], anti-seismic components for civil engineering structures [9], etc.

In more recent years a further promising field has been envisaged for NiTi materials, that could be employed as wear-resistant alloys. Several studies have been conducted on different systems, involving bulk alloys [10–16], coatings [17–22] and surface modified, e.g., ion-implanted, layers [23–32]. The tribological aspects of wear couples involving SMAs are attractive in several respects. Biomedical applications require the knowledge of mechanisms that may lead to the formation and release of wear debris. Friction may reduce the efficiency of the SMA-active components, by dissipating significant fractions of the work that can be produced by actuators and by hindering displacements in smart devices.

Another field in which the wear behavior of NiTi alloys may have a major importance is that of mechanical machining. As compared to other titanium alloys [33], NiTi materials have shown additional troublesome aspects [34, 35], mainly related to their relatively low thermal conductivity, low elastic moduli of both martensitic and austenitic polymorphs and elevated recoverable deformations. Therefore, the comprehension of the wear

S. Gialanella (✉) · G. Ischia · G. Straffelini
Dipartimento di Ingegneria dei Materiali e Tecnologie Industriali, Università degli Studi di Trento, Mesiano, Trento 38050, Italy
e-mail: stefano.gialanella@ing.unitn.it

mechanisms may help overcoming the still standing difficulties in mechanical machining NiTi alloys. Consequently, additional manufacturing tools would become available for these materials in addition to electrodischarge machining [36] and laser cutting [37].

The phenomenology of the SME and pseudoelasticity plays a major role in the tribological performances of NiTi alloys. Therefore, it is important to identify the actual state of the alloy material under the adopted tribological conditions.

The main aim of the present study is to characterize the dry-sliding wear behavior of martensitic and austenitic NiTi alloy samples. This comparative investigation intends to highlight how wear kinetics of the two NiTi alloys and of the counterface disk materials is influenced by the phase transitions induced in the alloys by test conditions, like applied load, frictional heating, etc.

Experimental

Two commercial NiTi alloy sheets have been acquired for the present research. The compositions and the thermomechanical treatments were such that one material, codenamed "A", having a composition Ni–44.08Ti (wt.%), is austenitic at room temperature and the other one, the "M" alloy, with a composition of Ni–44.67Ti (wt.%), is martensitic.

Differential scanning calorimetry (DSC) tests have been conducted on both materials to measure the relevant transition temperatures.

Mechanical tensile tests have been carried out on each alloy at different temperatures, selected on the basis of the calorimetric results, to measure the deformations and strengths characteristic of the austenitic and martensitic phases.

Vickers hardness tests, with a load of 30N, were conducted at room temperature on the alloy surface.

Wear tests were carried out in air at room temperature using an apparatus described elsewhere [38, 39], using a disk-on-block geometry under dry-sliding conditions. The sliding disk, having a diameter of 40 mm, was made either of AISI M2 steel, with hardness of 800 VHN or of a WC–Co alloy, with hardness of 1650 VHN. NiTi-alloy strips, 10-mm wide and 50–60-mm long, were used as "block" samples. The sample thickness was 1.25 mm for the M-alloy and 0.75 mm for the A-alloy. The sliding speed was 0.837 ms^{-1} corresponding to 400 rpm of the disk. A sliding distance of 1004 m for each run and applied loads ranging from 50 N to 200 N was adopted. The evolution of friction coefficient and temperature beneath the disk-block contact zone was recorded during the wear tests. At the end of each run, the weight loss of the worn samples was measured using a high-sensitivity precision balance.

The microstructure of the specimens was characterized with optical and environmental scanning electron microscopy (ESEM) observations, X-ray diffraction (XRD), using a monochromated CuKα radiation, and hardness tests. The low-vacuum operating mode employed for ESEM observations allowed us not to coat the specimen, that, as will be shown, occasionally contained insulating phases, e.g., oxides and carbides, with a conductive film. The composition of selected regions of the specimens was qualitatively evaluated with X-ray energy dispersive spectroscopy (EDXS).

Results

Alloy properties

In Table 1, the DSC results obtained with the two alloys are listed. According to these data, martensite phase, once it has been induced in the M-alloy by cooling it down below 10 °C (M_f), remains stable unless the material is not heated up above 70 °C, the austenite start temperature (A_s). The A-alloy has an austenite finish temperature (A_f) equal to 45 °C. The alloy remains in this phase down to −15 °C, the martensite start temperature (M_s).

Figure 1a shows the stress–strain curve for the A-alloy at room temperature. The curve displays a typical superelastic plateau, due to the austenite–martensite–austenite stress-induced transformations. The constant stress deformation is nearly fully recovered when unloading the tensile test specimen. The same alloy, when tested at a temperature in the martensite range (−50 °C) still displays a stress plateau, having a lower value than in the former case. This time the constant stress deformation is produced by the reorientation of martensite twins (detwinning) (Fig. 1b). Deformation is not recoverable just by unloading the sample, but a thermal treatment above the austenite transition temperature, exploiting the notorious one-way SME, would be required.

A similar tensile behavior is displayed by the M-alloy when tested at room temperature (Fig. 2a). Consistently with the DSC data, this same alloy tested at 100 °C, in a fully austenitic state, shows a superelastic behavior (Fig. 2b). Both alloys displayed at room temperature a

Table 1 DSC results for the two alloys: A_s = austenite start temperature; A_f = austenite finish temperature; A_p = austenite peak temperature; M_s = martensite start temperature; M_f = martensite finish temperature; M_p = martensite peak temperature

°C	A_s	A_f	A_p	M_s	M_f	M_p
Alloy A–NiTi	25	45	35	−15	−60	−35
Alloy M–NiTi	70	95	85	30	10	20

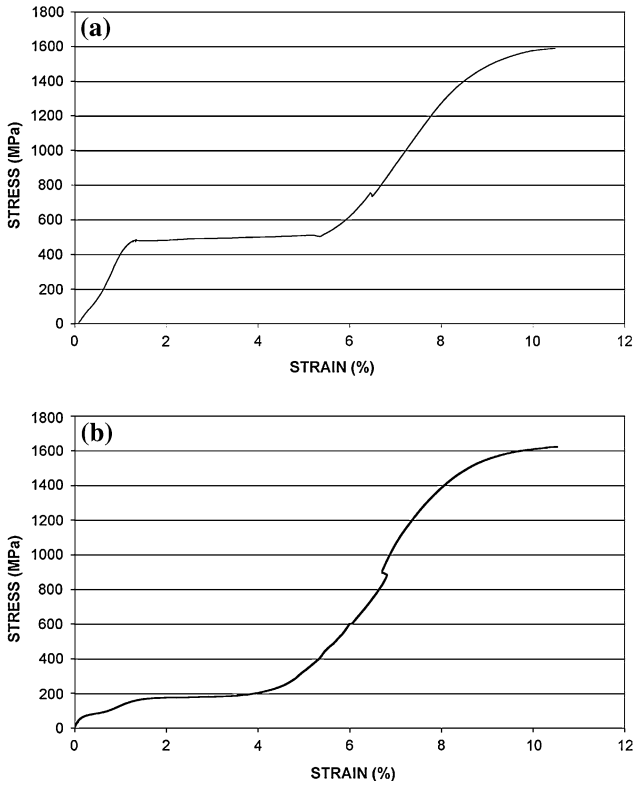

Fig. 1 Stress–strain curve for the A-alloy. (**a**) Room temperature, starting with a fully austenitic material. The constant stress plateau corresponds to the stress-induced austenite–martensite transformation; (**b**) −50 °C: the alloy is martensitic

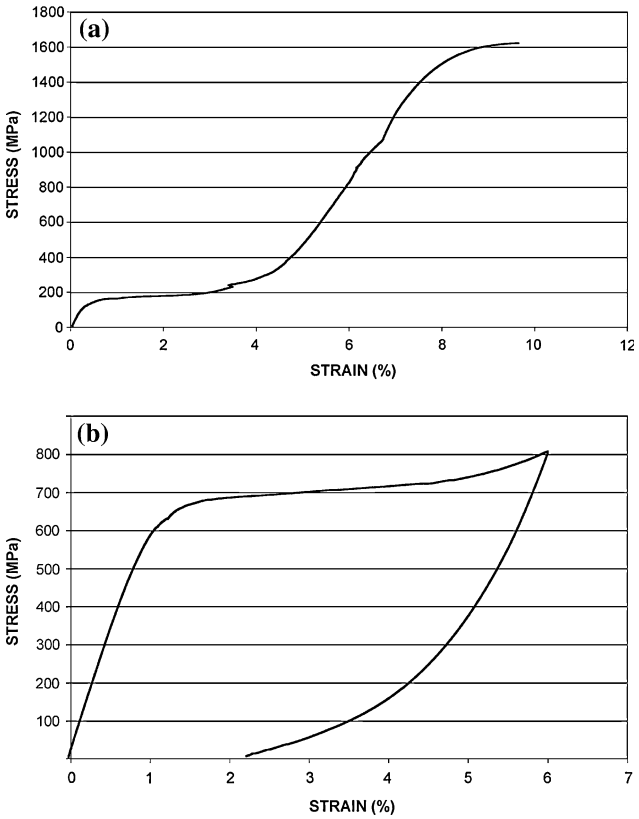

Fig. 2 Stress–strain curve for the M-alloy. (**a**) Room temperature, with a fully martensitic material. (**b**) At 100 °C: the alloy is in the austenite field

comparable deformation to fracture, equal to 10% approx. The fracture strength at room temperature of the two alloys also resulted to be the same. i.e., 1600 MPa. Room temperature hardness values for the two alloys are: 360 HV for the A-alloy and 235 HV for the M-alloy, with a standard deviation of 5% in both cases. The higher hardness value of the A-alloy is partly due to a more pronounced (super)elastic recovery that reduces the indentation size more than in the martensitic alloy.

Wear behavior

The dependence of the wear rate of the two NiTi alloys on the applied load during wear tests has been monitored through the normalized wear rate, or wear coefficient, K_A [40]. The normalized wear rate is defined, in terms of the wear rate W (volume of removed material versus sliding distance) and the applied load, L, as:

$$K_A = W/L.$$

This parameter is very effective in describing wear behavior of materials under different wear test conditions. In Fig. 3, the evolution of K_A with the applied load for the A and M alloys, dry-sliding against the AISI M2 steel disk, is shown. For both alloys all data points fall in the mild wear range. Moreover, both alloys display a reduction in the normalized wear rate when passing from 50 N to 100 N load. At higher loads, wear rate slightly increases, although for both materials it stays below the values measured at 50 N. It is worth noting that at 150 N and 200 N the M-alloy has a lower wear rate than the A-alloy, whereas in the low load range the two materials behave the same, within the limits of the experimental errors.

Significantly higher wear rates have been observed, over the same load interval, when alloy samples were sliding against a WC–Co disk. Figure 4 shows the K_A versus load curves for the two alloys. For a comparison the data points from Fig. 3, referring to the test conducted with the AISI M2 counterface disk, are displayed as well. With the harder WC–Co disk both alloys have wear rates one order of magnitude larger than with the AISI M2 steel, although still comparatively low. The general trend of the data points for the two alloys is comparable to what has been reported for the samples tested against the AISI M2 steel, with an initial decrease of K_A with the applied load. Wear rate of the A-alloy goes through a minimum and then starts increasing. For the considered values of the applied load no

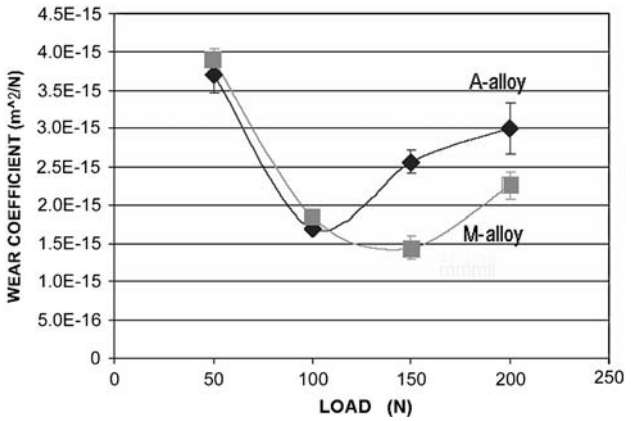

Fig. 3 Variation of the normalized wear rate, or wear coefficient, K_A, as a function of the applied load for the two NiTi alloys dry sliding against a AISI M2 counterface disk

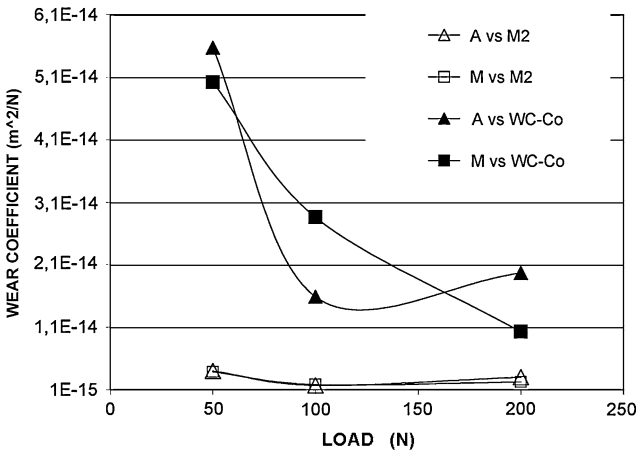

Fig. 4 Variation of the normalized wear rate, K_A, as a function of the applied load for the two NiTi alloys dry sliding against a WC–Co counterface disk. In the same plot the values for the NiTi-M2 wear couple (see Fig. 3) are displayed for a comparison

wear rate increase has been observed for the M-alloy, and that up to 200 N load continues to decrease. Another analogy that can be observed in the wear behavior of the two SMAs tested against two different counterface materials is the lower wear rate displayed by the M-alloy, as compared to the A-alloy, at the maximum load of 200 N.

Before moving on to the description of the experimental results concerning the microstructural characterization of the wear debris and tracks, a few notations on the wear behavior of the two counterface materials are worthwhile. The normalized wear rate of the AISI M2 disk as a function of the applied load is displayed in Fig. 5. The M2 steel displays a wear behavior that seems not to be sensitive to the different NiTi alloys, as the K_A values fall within the same range in both cases. Wear coefficients recorded for the steel disk are slightly higher than those of the alloys.

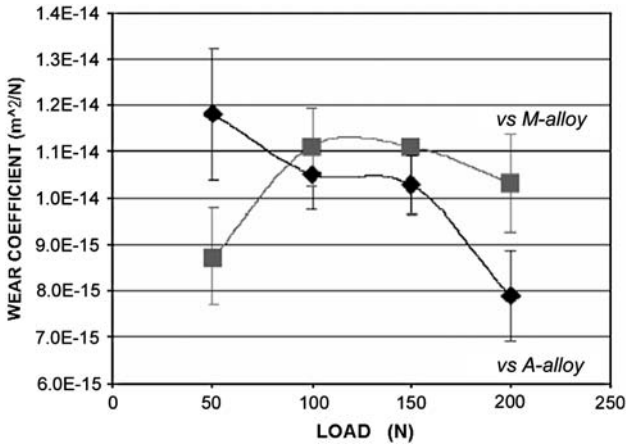

Fig. 5 Normalized wear rate, K_A, versus applied load for the AISI M2 counterface disk

The AISI M2 disk mating the M-alloy displays a K_A that goes through a maximum and then decreases. With the M-alloy all normalized wear rates are above those found with A-alloy samples, except that for the lowest load (50 N). With the A-alloy, the M2 counterface disk shows a continuous reduction in K_A as the load is increased.

Figure 6 shows the normalized wear rate versus load curves for the WC–Co material. In this case, a clear difference between the two tribological couplings, corresponding to the two NiTi alloys, can be noticed. The main difference with respect to the observations reported so far is the negative values of the normalized wear rate of the WC–Co disk.

Temperature and friction coefficient are very important parameters for the identification of wear mechanisms. They have been continuously recorded during the tests. In Fig. 7 the curves for the friction coefficient, μ, and temperature, T, recorded during a wear test conducted with a 50 N load and involving the A-alloy worn using an AISI M2 disk are displayed. The two curves display features that have been

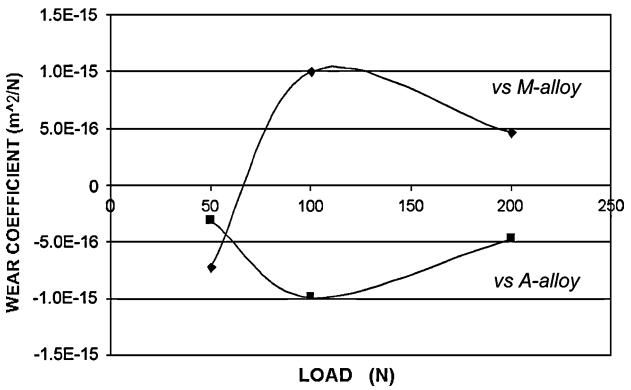

Fig. 6 Normalized wear rate, K_A, versus applied load for the WC–Co counterface disk

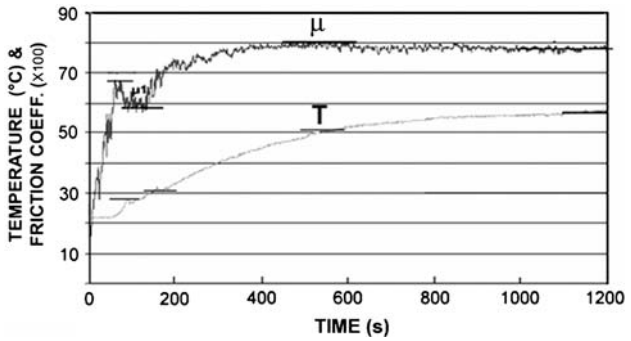

Fig. 7 Evolution of friction coefficient, μ, and temperature, T, as recorded during a wear test conducted with a 50 N load and involving the A-alloy worn using an AISI M2 disk

found qualitatively the same even under different experimental conditions. In particular, it is interesting to note that both friction coefficient and temperature evolve toward steady states, featuring comparatively stable values of the two parameters. The actual values of the stationary friction coefficients and temperatures will depend on the specific test conditions, as shown by the plots of temperature and friction coefficient versus load in Fig. 8a, b (see figure caption for the complete legend). From the plots in Fig. 8 it turns out that, for all wear couples that have been considered, temperatures increase with the load, whereas friction coefficients decrease.

Characterization of the wear products (NiTi versus AISI M2)

The mechanisms responsible for the observed wear kinetics have been investigated through the analysis of the wear tracks and debris obtained from the tests conducted under different conditions. From wear tests using AISI M2 steel as disk material two kinds of wear debris have been obtained. The first one corresponds to the descending part of the normalized wear rate curve in Fig. 3, i.e., to the loads of 50 and 100 N. In Fig. 9 an ESEM micrograph displays the typical morphology of this kind of wear debris produced by the A–NiTi alloy at 50 N. The EDXS analyses indicate that these wear particles are made of mixed oxides, containing mainly iron (from the sliding disk), nickel and titanium (from the alloy specimens). The submicrometric particles tend to stick together and form clusters that may abandon the tribological system. Alternatively, these clusters remain trapped in between the sliding surfaces and spread onto wear tracks. This is illustrated by Fig. 10, displaying the ESEM picture of the surface of a wear track on a M-alloy sample tested at 50 N. The brighter regions are parts of the NiTi alloy surface, on which the darker sintered oxide debris layers are clearly visible. These conditions are commonly encountered in tribological systems for which, we can conclude, oxidation is one of the dominant wear mechanisms

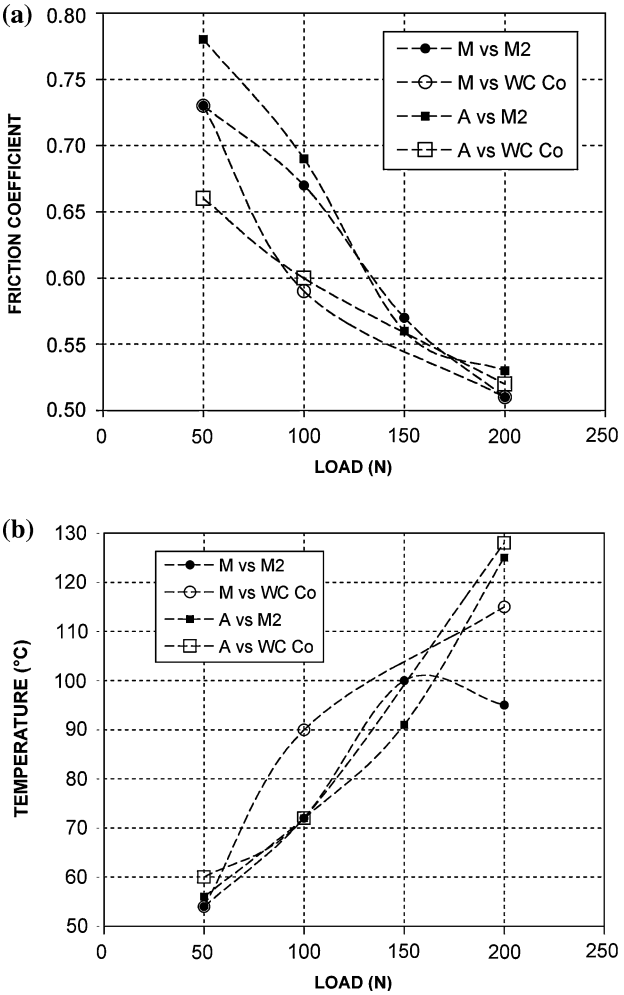

Fig. 8 Evolution of the steady state friction coefficient and temperature as a function of the applied load for the different wear test configurations adopted in the present study. (**a**) Friction coefficient for the A and M alloys sliding against AISI M2 and WC–Co disks. (**b**) Evolution of the temperature during the tests involving the above couplings

[41]. Similar microstructures as the one displayed in Fig. 10 have been observed in both NiTi alloys, M and A, wear tested at 50 and 100 N with the AISI M2 disk. This can be taken as an indication that the same wear mechanism is active under such experimental conditions.

At higher loads, corresponding to the ascending part of the normalized wear rate plot in Fig. 3, the situation is quite different. Wear debris, displayed in Fig. 11 and obtained from a test carried at 150 N with a M-alloy specimen, feature large NiTi alloy fragments partly covered with smaller particles, mainly made of iron oxides. Wear tracks on the NiTi alloys feature three distinct regions, as shown by Fig. 12 (alloy M tested at 200 N). We still have the sintered layers of mixed, mainly iron, oxides. Moreover, oxides are much thinner and appear to be intimately bound to the alloy surface over a significant area of

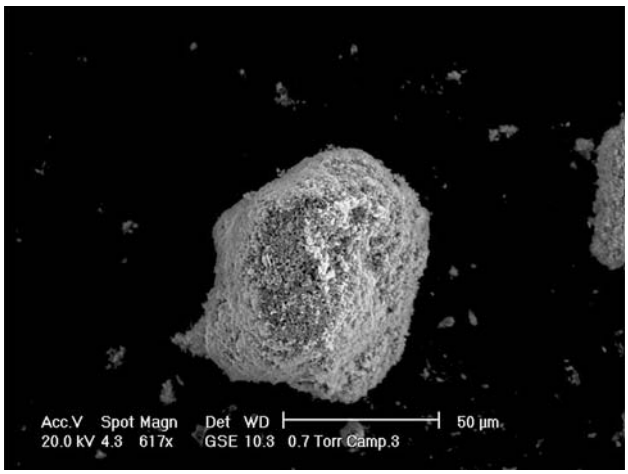

Fig. 9 ESEM micrograph displaying the microstructure of a cluster of wear debris particles collected at the end of the test conducted with the A–NiTi alloy versus AISI M2 wih an applied load of 50 N

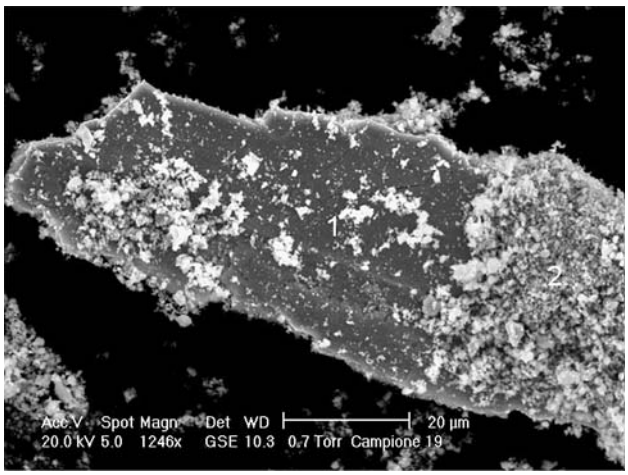

Fig. 11 ESEM micrograph displaying the typical microstructure of a wear debris collected at the end of a test conducted with the A–NiTi alloy versus AISI M2 with an applied load of 150 N

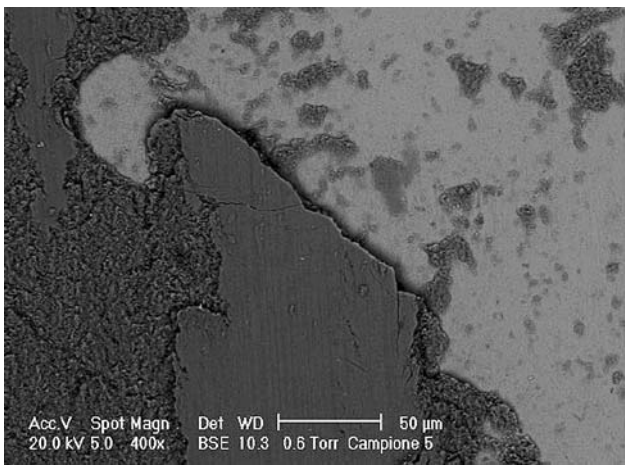

Fig. 10 ESEM micrograph showing the typical microstructure of a wear track observed on the M–NiTi alloy dry sliding against the AISI M2 disk with an applied load of 50 N

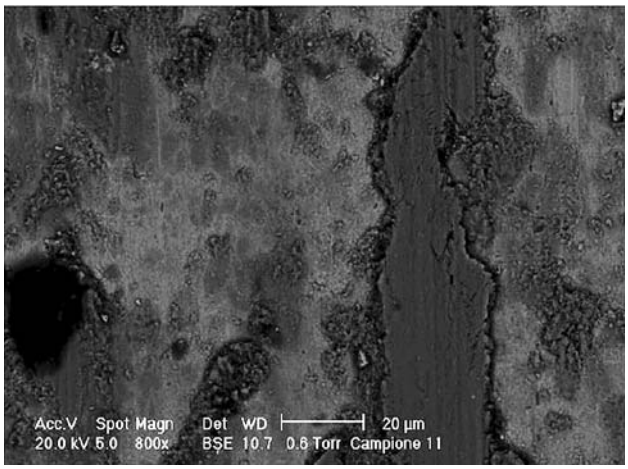

Fig. 12 ESEM micrograph showing the typical microstructure of a wear track observed on the M–NiTi alloy dry sliding against the AISI M2 disk with an applied load of 200 N

the track surface, owing to the higher applied pressures. Surface regions of the base alloy, appearing as brighter features in Fig. 12, are also visible in wear tracks. In view of the conditions of the nearby zones of the track surface, that, as just remarked, are covered with sintered oxide layers, it is plausible to think that the morphology of the wear tracks is the result of the delamination induced by heavy mechanical deformations.

Characterization of the wear products (NiTi versus WC–Co)

Delamination is the main wear mechanism in wear tests conducted at the low load (50 N) using WC–Co as counterface disk material. Wear debris obtained from the M–NiTi alloy mainly consist of NiTi lamellar fragments (Fig. 13), with smaller particles identified as nickel and titanium oxides. Compacted oxide layers have been observed on the wear tracks. In Fig. 14, the morphology of wear tracks on the M-alloy tested at 50 N is shown. In this case too, as already seen in Fig. 12, the light gray regions are freshly created surfaces of the base alloy, appearing once fragments have been removed from the surface of the specimen. Another interesting feature of the low load wear tracks is the presence of tungsten carbides, the bright particles scattered on the surface of the wear tracks. These carbides come from the counterface disk, indicating that a good adhesion is established between the two mating surfaces of the NiTi alloy and the disk. The situation described

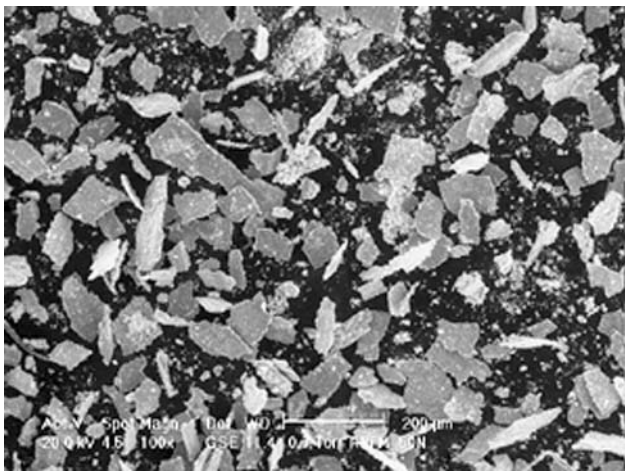

Fig. 13 ESEM micrograph displaying the microstructure of wear debris particles collected at the end of a test conducted with the A–NiTi alloy versus WC–Co with an applied load of 50 N

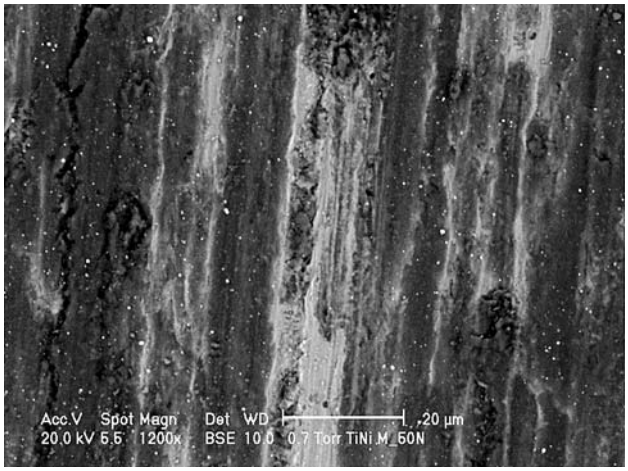

Fig. 14 ESEM micrograph showing the typical microstructure of a wear track observed on the M–NiTi alloy dry sliding against the WC–Co disk with an applied load of 50 N. Brighter particles are tungsten carbides

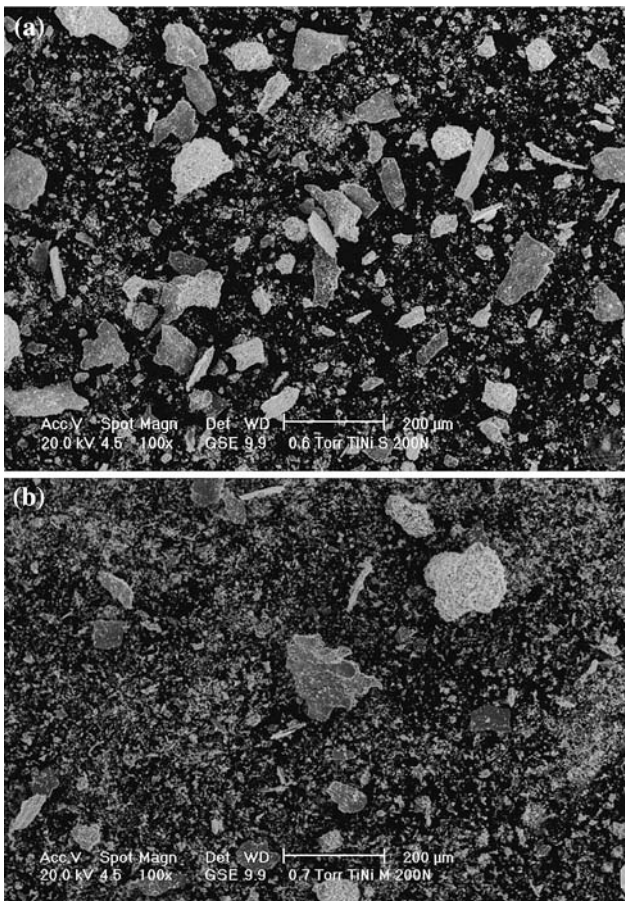

Fig. 15 ESEM micrographs displaying the microstructure of wear debris particles collected at the end of a test conducted with the NiTi alloy sliding against WC–Co with an applied load of 200 N. (**a**) A–NiTi alloy; (**b**) M–NiTi alloy

so far, as concerns both wear debris and tracks, is pretty much the same in the case of the A-alloy. Therefore, it can be assumed that the dominant wear mechanisms are the same for both NiTi alloys.

At higher loads wear debris is characterized by a higher concentration of nickel and titanium oxide particles (Fig. 15a, b), as resulted from a comparison of EDXS spectra corresponding to a wide field of view. As to the corresponding wear tracks, they alternate alloy free surface regions and layers of compacted oxide particles (Fig. 16a, b). These layers have larger size on the surface of the A-alloy (Fig. 16a), while they look thinner and not so wide on the surface of the M-alloy (Fig. 16b).

Discussion

In this study, the behavior of two NiTi SMAs has been considered. One of the NiTi alloy is austenitic the other one martensitic at room temperature. The actual phase composition of each alloy and its dependence on temperature has important effects on the mechanical response of the shape memory materials, as clearly shown by the results of tensile tests (Figs. 1 and 2) carried out on the NiTi alloys at temperatures selected on the basis of calorimetry results (Table 1).

The dry sliding wear tests of the two NiTi alloys displayed similar trends as concerns wear coefficient as a function of the applied load. In both Figs. 3 and 4, an initial decrease in K_A is observed. However, the microstructural investigations on the wear products indicate that the phenomena responsible for this similar wear behavior are not quite the same for the two materials used as counterface disk: the AISI M2 steel and the WC–Co alloy. In case wear tests were conducted using the AISI M2 steel slider, wear

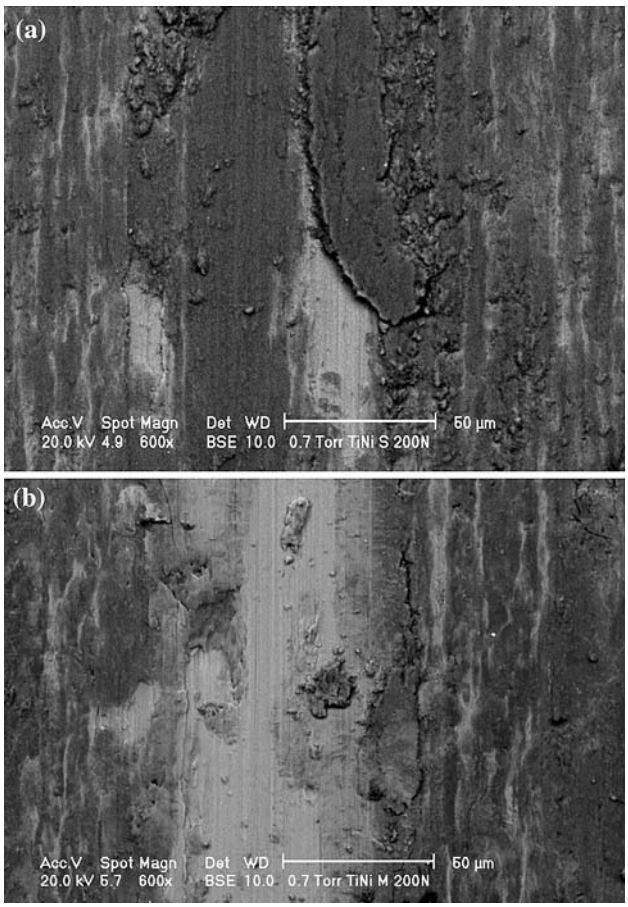

Fig. 16 ESEM micrographs showing the typical microstructure of a wear track observed on the NiTi alloys dry sliding against the WC–Co disk with an applied load of 200 N. (**a**) A–NiTi alloy; (**b**) M–NiTi alloy

debris is made of mixed oxide particles containing elements from the steel disk mainly and, to a lower extent, of the NiTi alloys (Fig. 9). We propose that the oxidation process is triggered by the formation of particles of the NiTi alloys. These alloys, being significantly softer than the M2 steel, are easily abraded by the refractory element carbides present in the steel. For instance, the micrometric abrasion traces of the carbides are visible on the sintered oxide layer in Fig. 10. Owing to the elevated reactivity of nickel and, even more, titanium, metallic fragments get easily oxidized and start abrading the M2 disk. This phenomenon corresponds to the run-in stage of the friction coefficient versus time curves (see for instance Fig. 7). Oxide particles are present to an increasing extent between the sliding surfaces as wear test proceeds. Unless they abandon the systems, these oxide particles start compacting and sintering, and build up mixed protective layers on the alloy surface (Fig. 10). This stage is marked by a reduction in the friction coefficient, observable in the relevant curves. The higher the applied load, i.e., 100 N versus 50 N, the quicker is the formation of protective compacted oxide layers. This also results in a reduction in K_A, when passing from 50 N to 100 N load. At higher loads (150 and 200 N), oxidation is still occurring to some extent, as proved by the observations on the wear products. However, the tribological coupling is now dominated by a strong adhesion between the M2 disk and the compliant alloy specimens. Adhesion and surface strain-hardening of the NiTi samples are responsible for the delamination of the alloy samples, resulting in the formation of larger metallic alloy debris (Fig. 11). The contribution of two main wear mechanisms, oxidation and delamination, is nicely confirmed by the morphology of the wear tracks (Fig. 12), displaying the alternate presence of layers of compacted oxide particles and alloy-free surface regions from which the metallic debris has been removed.

The observed increase in the wear coefficient (Fig. 3) is actually in agreement with the evolution of the steady friction coefficient as a function of the applied load (Fig. 8a). In fact, strain hardening of the outer alloy layers would actually reduce the adhesive contribution, μ_{AD}, to the overall friction coefficient through the following relationship [42]:

$$\mu_{AD} = \tau_m/H$$

where τ_m is the shear strength of the alloy-slider junction and H is the alloy surface hardness. Surface hardening has also beneficial effects on the resistance to abrasive wear of the NiTi alloys. In our case, a major contribution to abrasive wear comes from the high concentration of carbides in the AISI M2 steel. It is interesting to note that, differently from literature findings [10, 43], in the high-load region, in which adhesion is dominating the wear behavior of the NiTi-M2 couple, the martensitic alloy displays a better wear resistance than the austenitic material. The elevated deformations at constant stress that NiTi alloys are capable to sustain in the martensitic and austenitic fields, through the mechanisms of detwinning and of the stress-induced martensitic transformation, respectively, are regarded as the main factors that determine the excellent wear performances of these alloys.

In case of SMA specimens deformed in the martensitic field, their initial austenitic shape can be recovered upon heating them up at temperatures higher than the relevant austenite finish temperature (A_f, see Table 1). In the present study, it can be inferred that the NiTi alloy wear debris, worn out from both A and M alloys, has been deformed in the martensitic state. For the M alloy this occurs in view of the temperatures reached during wear tests at lower loads. At the higher loads (Fig. 8b), temperatures in excess of austenite finish ($A_f = 95$ °C) are achieved and the alloy might actually become austenitic. However, also in this condition, for the elevated accumulation of deformation, proved by a diffuse cracking of the alloy, stress-induced

martensite phase transformation might occur. Therefore, also wear debris produced at this stage would behave very similar to the ones that formed at temperatures falling in the martensite field. The A-alloy sample too may be taken to the stress-induced martensite field when sufficiently high deformations have been achieved. In view of this scenario, we propose that, as displayed in Fig. 4, the higher wear rate of the A-alloy depends on an earlier achievement, than in the M-alloy, of temperatures in excess of its austenite finish temperature ($A_f = 45$ °C), owing to frictional heating associated with wear tests. Above this temperature, alloy debris would detach from the disk, and then leave more easily the tribological system, as a result of the SME that would take the alloy fragments back to the original flat shape they had in the sheet. As the M-alloy has a significantly higher austenite transition temperature, $A_f = 95$ °C, the detachment of the debris from the disk can only take place at higher temperatures, reached after longer times. However, this is the main but not the only reason why wear rate of the M-alloy turns out to be lower than that of the A-alloy under the present wear conditions. To complete the picture it should be considered that the spring-back energy available for the detachment of the metallic debris is to some extent proportional to the area of the relevant stress–strain curves. The A-alloy is capable to store increasingly higher amounts of energy from room temperature upward, once the deformation to fracture has been overcome (Fig. 1a). In fact, the stress at which the superelastic deformation plateau starts increases with temperature. For the M material the "elastic" energy stored at room temperature is comparatively smaller (Fig. 2a). Only when the alloy is transformed back to the austenitic phase (Fig. 1b) the energy available for the spalling of the debris is comparable to that of the A-alloy.

Although some similarities, in terms of the variations of friction coefficients, temperature (Fig. 8) and wear rate (Fig. 4) as a function of the applied load, have been observed in the wear behavior of the NiTi/WC–Co and NiTi/M2 systems, the active wear mechanisms are quite different. The decrease in the wear rate of both NiTi alloys, dry sliding against the WC–Co disk, with increasing loads is determined by the transition from a regime in which abrasion is the main mechanism toward a condition in which some oxidation too occurs. Abrasion, that induces the formation of metallic debris, is mainly due to tungsten carbides that are removed from the metallic cobalt matrix and act as third bodies trapped between the mating surfaces (Fig. 15). As the counterface disk in much harder than the NiTi alloys, carbides can be implanted into the surface of the alloys or being embedded inside the layers of compacted debris, as shown by Fig. 14. As loads are increased, the more demanding wear conditions, particularly the higher temperatures, induce the formation of protective oxide layers, through the compaction of wear debris (Figs. 15 and 16). These layers reduce the abrasive action of the carbides, resulting in lower friction coefficients (Fig. 8) and wear losses (Fig. 4).

As concerns wear behavior of the two counterface disk materials, they turned out to be rather different under different dry sliding conditions. Wear rates measured for the M2 steel fall in the same range as the two NiTi alloys. Moreover, for all loads, but the lower one, i.e., 50 N, the M2 material has comparable and nearly constant wear rates, irrespective of the SMA (see Fig. 5). At 50 N, a better wear resistance of the M2 mating the martensitic alloy, as compared to M2 versus the austenitic one, is to be ascribed to the lower friction coefficient that has been measured for the M2/NiTi M alloy (Fig. 8a). This lower friction coefficient would actually correspond to lower real shear stress acting on the two surfaces in contact. For a given load, real stress can be reduced by an increase of the real contact area. This condition can be fulfilled to a larger extent by the M-alloy for two main reasons. The M-alloy is softer than the A-alloy. Moreover, the rearrangement of the martensitic variants, resulting in the constant stress deformation plateau observed in the stress–strain curves, occurs at a significantly lower stress than in the case of the A-alloy (see curves in Fig. 2a and Fig. 1a, respectively).

As to the wear rate of the slider at higher loads, the monotonic slowing down that has been recorded can be safely ascribed to an increasingly protective action provided by the layer of the compacted wear debris [44]. As already discussed with reference to the NiTi alloys, debris that get trapped in between the block and the disk are oxidized and then compacted onto the surface of the wear tracks (Fig. 12). In all cases, from 50 N up to 200 N, iron oxide particles have always been found in the wear debris. This suggests that oxidation promotes and/or assists wear kinetics of the M2 disks.

As to the WC–Co hard-metal sliders, very low wear rates have been measured, much lower than that for the M2 steel and, thereby, of the two NiTi alloys (Fig. 6). Negative values of the wear coefficient, resulting from the adhesion of wear debris onto the slider surface, have been measured. This effect is more pronounced in the softer M-alloy. As already stated, the ubiquitous presence of tungsten carbides, directly inserted into the alloy or on the compacted layer of wear debris, has been observed at 50 N. These particles, particularly those more loosely bound to the Co matrix, at different stages of the wear process are removed. In particular, when disk and block metallic surfaces are in contact, tungsten carbides adhere to NiTi and are removed by the shear stress resulting from sliding. At later stages of the test, or under more severe conditions, when significant amounts of oxide debris are present, even an abrasive removal of carbides may occur.

Conclusions

A large number of literature studies have shown the potentially interesting properties of NiTi SMAs for tribological applications. In the present research wear behavior of two of these alloys, dry sliding against an AISI M2 steel and a WC–Co hardmetal counterbody, has been investigated to understand how different phase compositions may affect wear kinetics of these materials.

A general result is a comparable, or possibly better, wear resistance of the martensitic alloy, as compared to the austenitic one. Different wear mechanisms are active under different wear conditions. With the M2 steel counterface disk, in the lower load region (50–100 N) oxidation is largely dominating wear kinetics and the two alloys behave all the same. This is not unexpected, as the frictional heating takes the martesitic alloy into the austenitic field since the early stages of wear tests. At higher loads, delamination, with the formation of metallic debris becomes increasingly important. At this stage the martensitic alloy has a lower wear rate than the austenitic one. For the latter, in fact, wear debris recovers the original flat geometry for the SME and would therefore tend to detach from the mating surfaces, thus increasing wear rate. This phenomenon, induced by the one-way-shape-memory effect, happens to a lower extent in the martensitic alloy, having a higher austenite transition temperature. With the WC–Co counterbody, the sequence of wear mechanisms taking place at increasing loads is rather different. As WC–Co is significantly harder than the NiTi alloys, higher wear rates of the SMAs have been observed with the NiTi/WC–Co couple. In this case a transition from a mainly delamination wear to a regime featuring a mixture of delamination–oxidation wear has been observed. The hard metal disks present an extremely low wear rate, mostly determined by the loss of tungsten carbides that are extracted from the disk mainly by the intense adhesive interaction with the NiTi alloy.

As a general comment to the observed results, it can be concluded that wear mechanisms intervening in material couples involving SMAs are very much dependent on the actual response they display under different thermal, mechanical and environmental operating conditions.

Acknowledgements We wish to thank Dr. M. Piotto and Dr. M. Mazzanti for their valuable contribution to the present work. We also thank W. Vaona for DSC analyses, A. Casagranda for tensile tests, and C. Bressanini for ESEM observations respectively.

References

1. Duerig TW, Melton KN, Stockel S, Wayman CM (1990) Engineering aspects of shape memory alloys. Butterworth Heinemann, London
2. Van Humbeeck J (1999) Mater Sci Eng A A273–A275:134
3. Lipscomb IP (1996) The application of shape memory alloys in medicine. Paston Publ., London
4. Oshida Y, Sachdeva R, Miyazaki S, Fukuyo S (1990) Mater Sci Forum 56–58:705
5. Oshida Y, Miyazaki S (1991) Corros Eng 40:1009
6. Busch JD (1994) In: Proceedings of the First International Conference on Shape Memory and Superelastic Technologies, Pacific Grove, Ca, 1994. SMST Intnl. Comm. Publ., New York, p 259
7. Zhang X, Nie J, Hou G (2000) Mater Sci Forum 327–328:35
8. Bellouard Y (2002) In: Schwartz M (ed) Encyclopedia of smart materials, vol 2. Wiley, New York, pp 620–644
9. Adachi Y, Unjoh S, Kondoh M (2000) Mater Sci Forum 327–328:31
10. Li DY (1996) Scripta Mat 34(2):195
11. Qian LM, Sun QP, Zhou ZR (2005) Tribol Lett 18(4):463
12. Richman RH, Kung D, Rao AS (1995) Wear 181–183:80
13. Lin HC, Wu SK, Yeh CH (1991) Wear 249:557
14. Imbeni V, Martini C, Prandstaller D, Poli G, Trepanier C, Duerig TW (2003) Wear 254:1299
15. Li DY (2003) Wear 255:617
16. Qian L, Zhou Z, Sun Q (2005) Wear 259:309
17. Wang HM, Cao F, Cai LX, Tang HB, Yu RL, Zhang LY (2003) Acta Mat 51:6319
18. Paro JA, Gustafsson TE, Koskinen J (2004) J Mater Process Technol 150:309
19. Paro JA, Gustafsson TE, Koskinen J (2004) J Mater Process Technol 153–154:622
20. Bram M, Ahmad-Khanlou A, Buchkremer HP, Stöver D (2002) Mater Lett 57:647
21. Wang HM, Liu YF (2002) Mater Sci Eng 338:126
22. Ni W, Cheng Y-T, Lukitsch M, Weiner AM, Lev LC, Grummon D (2005) Wear 259:842
23. Tan L, Crone WC (2002) Acta Mater 50:4449
24. Cui ZD, Man HC, Yang XJ (2003) Appl Surf Sci 208–209:388
25. Tan L, Crone DA, Crone WC (2003) Biomaterials 24:3931
26. Sridharan L, Sridharan WC, Sridharan K (2002) J Mater Sci Mater Med 13:501
27. Wu SK, Lin HC, Lee CY (1999) Surf Coat Technol 113:13
28. Pelletier H, Muller D, Mille P, Grob JJ (2002) Surf Coat Technol 158–159:301
29. Pelletier H, Muller D, Mille P, Grob JJ (2002) Surf Coat Technol 158–159:309
30. Lin HC, Liao HM, Lin KM, He JL, Chen KC (1997) Surf Coat Technol 92:178
31. Wu SK, Lin HC, Chu CL (1997) Surf Coat Technol 92:206
32. Tan L, Shaw G, Sridharan K, Crone WC (2005) Mech Mater 37:1059
33. Ezugwu EO, Wang ZM (1997) J Mater Process Technol 68:262
34. Lin HC, Lin KM, Chen YC (2000) J Mater Process Technol 105:327
35. Weinert K, Petzoldt V (2004) Mater Sci Eng 378:180
36. Lin HC, Lin KM, Cheng IS (2001) J Mat Sci 36:399
37. Rohde M, Schussler A (1997) Sens Actuators A 61:463
38. Straffelini G, Dorigatti R, Gialanella S (1998) Mater Sci Technol 14:143
39. Gialanella S, Straffelini G (1999) Met Mater Trans A 30A:2019
40. Ashby MF (1992) Materials selection in mechanical design (Materials and process selection charts). Pergamon Press, Oxford, p 36
41. Stott FH, Wood GC (1978) Tribol Int 14:123
42. Hutchings IM (1992) Tribology. Edward Arnold Publ., London
43. Li DY (1998) Wear 221:116
44. Rabinowicz E (1995) Friction and wear of materials, 2nd edn. Wiley, New York